

Final Performance Report for Grant # FA9550-08-1-0329

Program Manager: **Dr. Byung-Lip Lee**

Grant/Contract: **Electromagnetically Tunable Fluids**

PIs: **G. H. Huff, M. A. Bevan, Z. Ounaies, J. Boyd, and D. Lagoudas**

Reporting Period: **01-JUL-2008 to 31-AUG-2011**

A. Project Summary

The overarching goal of this project was to exploit the transport properties at colloidal and microfluidic dimensions to controllably alter the high-frequency electromagnetic material properties at the macro level. This was to achieve multifunctionality and reconfigurability at device-level (antenna) scales through tunability provided by a combination of structural colloidal components and functional microfluidic components; the microfluidic system was used to both reversibly control physical properties through fluidic transport and provide pathways for directed colloidal assembly. A series of multidisciplinary activities have been completed to explore these adaptive properties and integrate them into the design of a demonstration vehicle. This includes a combination of microscopy, numerical simulation, scaling analysis, and image analysis which has been used to evaluate and model the multi-body forces acting within the colloidal assemblies and fluidic dispersions. New synthesis procedures were developed to provide nano-scale material systems with high aspect ratio particles and test fixtures were developed for the high frequency electromagnetic characterization of these materials. Multi-scale multi-physics modeling was also examined to provide additional insight into the interconnection of physical phenomena that were associated with multifunctional behavior of the antenna systems.

B. Project Accomplishments

1. *Colloidal Assembly: Exploit and tune transport properties of various colloids to controllably adjust their electromagnetic response at the macro-scale*

i. Microfluidic pressure driven flows within quasi-2D microfluidic networks

The microfluidic pressure driven flow within several quasi-2D microfluidic networks with integrated metallic electrodes has been investigated in this project. Fig. 1 shows four examples of activities in this area which were modeled using COMSOL to evaluate the impact of non-planar geometries and to enhance the gradient of the electric field in the device and influence the Maxwell stress tensor. All four of these plots show a color-mapped view of the electrostatic field which transitions from a +1 Volt excitation in red and -1 Volt excitation in blue; the black arrows in these plots represent the resulting dielectrophoresis force-field resulting from the applied electric field that are acting on the fluid within the device. The top-left side of this figure shows a non-planar potential-well with bias applied to the top and bottom sides (the bottom includes a long narrow tube with a curvilinear pit at the bottom); the purpose of this topology is to create a non-uniform gradient of the electric field along the bottom of a uniform channel to migrate and trap particles (to alter the effective constitutive properties of the dispersion). The top-right side of this figure shows a forked fluidic channel with electrodes on the outer edges of both the right and left fork; this Y-splitter was examined to study the control of spatial

Report Documentation Page				Form Approved OMB No. 0704-0188	
Public reporting burden for the collection of information is estimated to average 1 hour per response, including the time for reviewing instructions, searching existing data sources, gathering and maintaining the data needed, and completing and reviewing the collection of information. Send comments regarding this burden estimate or any other aspect of this collection of information, including suggestions for reducing this burden, to Washington Headquarters Services, Directorate for Information Operations and Reports, 1215 Jefferson Davis Highway, Suite 1204, Arlington VA 22202-4302. Respondents should be aware that notwithstanding any other provision of law, no person shall be subject to a penalty for failing to comply with a collection of information if it does not display a currently valid OMB control number.					
1. REPORT DATE 29 NOV 2011		2. REPORT TYPE		3. DATES COVERED 01-07-2008 to 31-08-2011	
4. TITLE AND SUBTITLE Electromagnetically Tunable Fluids				5a. CONTRACT NUMBER	
				5b. GRANT NUMBER	
				5c. PROGRAM ELEMENT NUMBER	
6. AUTHOR(S)				5d. PROJECT NUMBER	
				5e. TASK NUMBER	
				5f. WORK UNIT NUMBER	
7. PERFORMING ORGANIZATION NAME(S) AND ADDRESS(ES) Texas Engineering Experiment Station ,TAMUS 3000,College Station,TX,77843				8. PERFORMING ORGANIZATION REPORT NUMBER	
9. SPONSORING/MONITORING AGENCY NAME(S) AND ADDRESS(ES)				10. SPONSOR/MONITOR'S ACRONYM(S)	
				11. SPONSOR/MONITOR'S REPORT NUMBER(S)	
12. DISTRIBUTION/AVAILABILITY STATEMENT Approved for public release; distribution unlimited					
13. SUPPLEMENTARY NOTES					
14. ABSTRACT					
15. SUBJECT TERMS					
16. SECURITY CLASSIFICATION OF:			17. LIMITATION OF ABSTRACT Same as Report (SAR)	18. NUMBER OF PAGES 27	19a. NAME OF RESPONSIBLE PERSON
a. REPORT unclassified	b. ABSTRACT unclassified	c. THIS PAGE unclassified			

displacement on specific particles as an embedded particle extraction mechanism (e.g., the volume fraction in this device is reduced by forcing the particles down different paths of the fork, and different voltages control where the particles flow). The bottom of this figure shows two variations on a rectangular channel similar to the top-left structure with a curvilinear channel; however, the width of the channel has been studied to test the effectiveness of multiple height-to-width ratios on the resulting fields and their ability to influence the forces on particles. These devices were not fabricated, but their study illustrates the process for multi-physics modeling within the microfluidic device.

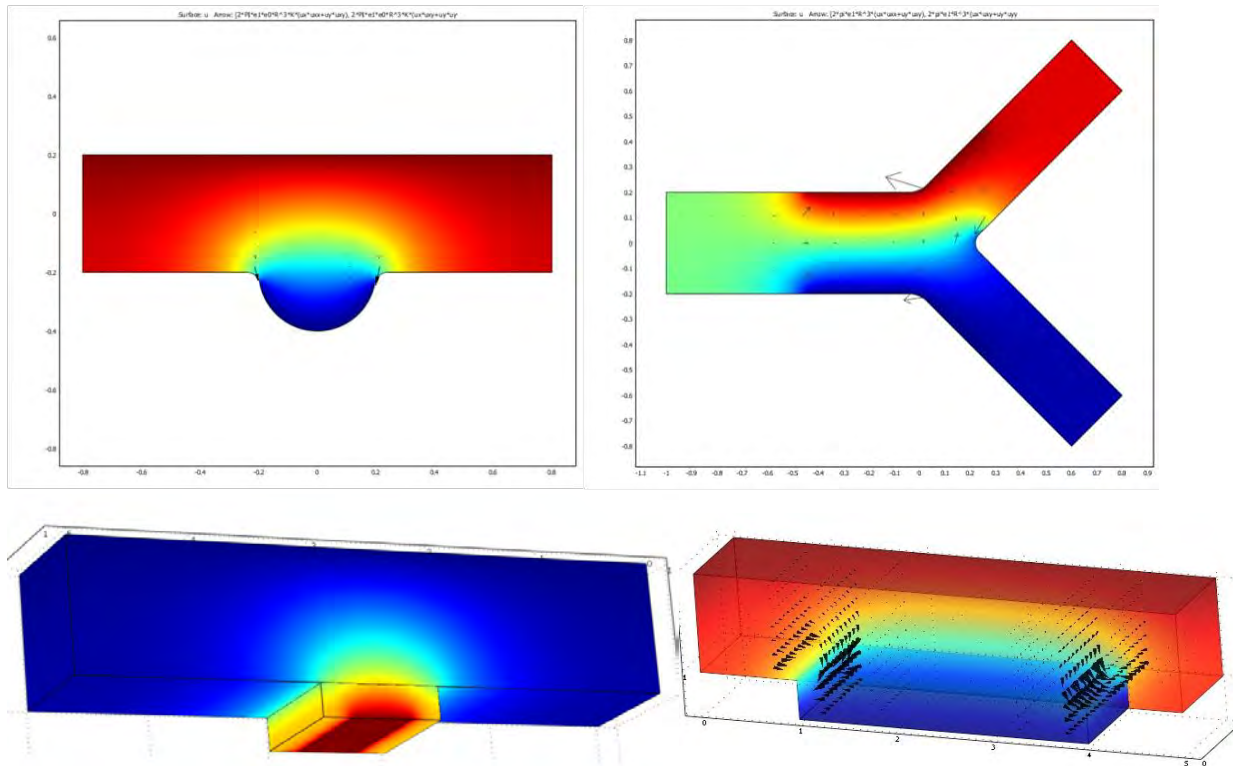


Fig. 1 – A long narrow tube with a curvilinear pit at the bottom to create a non-uniform gradient of the electric field to trap particles (top-left), a forked channel to control the spatial displacement of specific particles as an embedded structure within the antenna or other device (top-right), and two rectangular variations of the particle trap to study the impact of channel depth, electrode width, and overall size of the fluidic network.

Multi-physics simulations were also performed to better understand the process of manipulating particle dispersions through transient fluidic flow in the pressure-driven system. This behavior remains critical to overall performance and longevity of any electromagnetic device using this type of system so the movement of a single particle being pumped through a curve in a capillary system was analyzed as a benchmark for this. It has a practical goal of also ensuring there is no (or minimal) particle sedimentation throughout the capillaries; hence, the geometry of interest for the fluid dynamics is the 90° bend, which was chosen because the capillary system used later in the reconfigurable antenna has three such bends (and two more which are more shallow). These are the most likely areas for sedimentation and other aggregation so the Incompressible Navier-Stokes and Moving Mesh modules of COMSOL were used to solve this problem numerically. Each of the simulation results shown in Fig. 2 represent a snapshot in time of this topology using a 1 μm diameter particle (in white) in the 5 μm wide

curved capillary. Thus, once a simulation converged to a solution the forces on the particle were calculated and it was moved according to the calculated acceleration and velocity changes. The simulation starts with no fluid flow at time $t = 0^+$ s (left) and ramps up to a steady-state flow rate of 1 mL/s at $t = 30$ s (right) according to a time-dependent relationship; the colors indicating the velocity from high (red) to low (blue). Similar simulations were used to verify that the capillary networks used in reconfigurable antenna design would not create unintentional particle traps which could lead to device failure or a reduced performance.

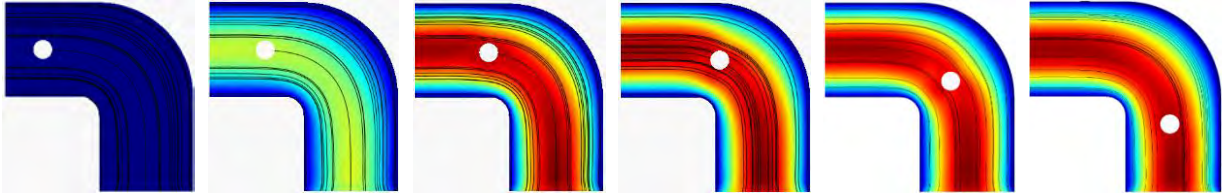


Fig. 2 – Snapshots in time of transient moving-mesh fluid dynamics simulations for a 1:5 particle-to-capillary ratio in an incompressible fluid.

ii. Integration of electrical and microfluidic networks to tune local material EM properties through electric field directed colloidal assembly

Understanding and modeling the frequency response of dilute dispersions of colloids in externally applied AC electric fields is important for designing, controlling and optimizing emerging particle based devices. It represented a major focus of this project so making the connection between modeling, simulation, and measurements was a critical step in this process. To accomplish this, measurements of the lateral potential energy distribution for a single particle in a non-uniform AC field were examined using video microscopy. These demonstrated that Diffusing Colloidal Probe Microscopy (DCPM) is a practicable method for mapping particle-field interaction potentials and understanding the interaction. Predictions of potential energy wells are consistent with observed position distribution for various sized SiO_2 particles in different AC electric field strength regimes. The DCPM technique was adapted to investigate the frequency dependence of polystyrene particles. This measurement allowed for an accurate estimate of the crossover frequency and suggested that the particle conductivity could be measured directly at low frequencies.

The model developed in this project can be employed to predict the frequency-actuated colloidal particle assembly (induced by an external field) for the controlled and tunable growth of colloidal crystals. Fig. 3 illustrates some of the results obtained from this focus of the project. The top left of this figure shows a top view and a Persistence of Vision Raytracer (POV-Ray) rendering side view of the experimental cell showing a Polydimethylsiloxane (PDMS) ring and DI water sealed by a cover slip. The top right provides a video microscopy image of a single SiO_2 colloid (with a $3.01\ \mu\text{m}$ diameter) diffusing between $30\ \mu\text{m}$ thin film coplanar electrode gaps. The bottom left shows the XZ cross-section of the net potential energy ($u^{net} - u_{min}$) on a linear scale from $0\ \text{kT}$ – $6\ \text{kT}$ for a single SiO_2 (diameter $2.34\ \mu\text{m}$) colloid in a 2 V, 1MHz AC electric field. The bottom right of the figure shows the trajectory of an SiO_2 (diameter $3.01\ \mu\text{m}$) colloid in a 2 V, 1MHz AC electric field captured using video microscopy (linear color scale, 0 – 30 minutes). These represent a significant advance in the modeling capabilities for these colloidal material-based systems.

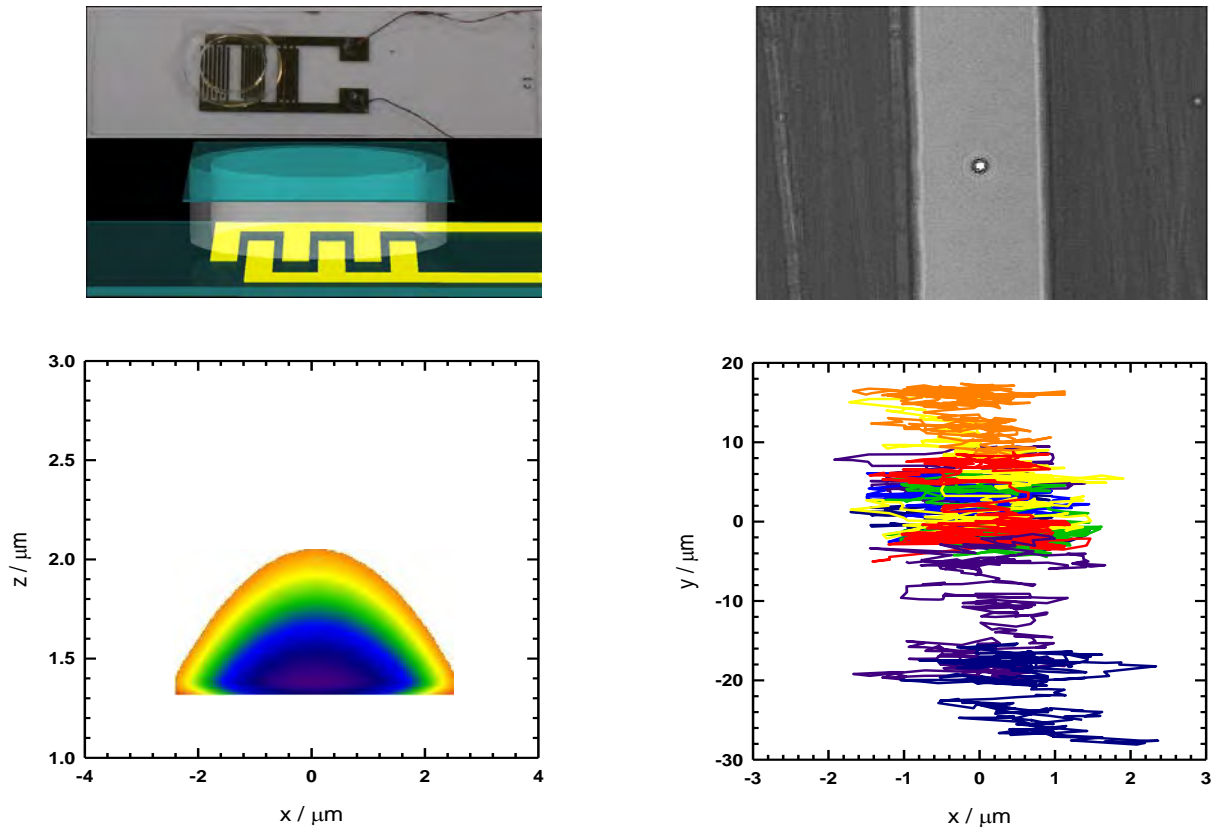


Fig. 3 – Frequency-actuated colloidal particle assembly in an external field.

Fig. 4 provides a sample of the modeling process using this trajectory data (from Fig. 3) to illustrate the use of this modeling technique. This figure shows the one-dimensional dielectrophoretic potential energy calculations from histograms of trajectory data of SiO_2 diffusing colloidal probes in a $30\ \mu\text{m}$ electrode gap for amplitudes of $0.5\ \text{V} - 2\ \text{V}$ at a constant frequency of $1\ \text{MHz}$. The experiments were carried out for $1.59\ \mu\text{m}$ SiO_2 colloids (purple circle: $2\ \text{V}$, indigo triangle: $1.5\ \text{V}$, blue square: $1.0\ \text{V}$, green diamond: $0.5\ \text{V}$), and all show good agreement with the models derived from DCPM observations.

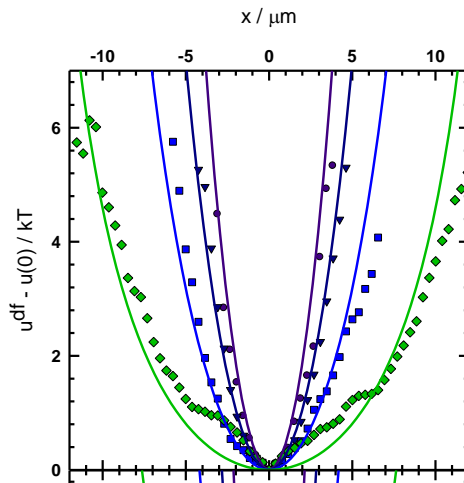


Fig. 4 – Frequency-actuated colloidal particle assembly in an external field.

Fig. 5 illustrates the use of new electrode geometries in this project, and represents converging work towards the understanding of electrokinetic behavior and its application to high frequency devices (antennas, etc.). The top left of this figure shows a POV-Ray rendering which illustrates the experimental quadrupole device used in experiment and the bottom left shows a photograph of the experimental quadrupole device showing the soldered leads connected to each pole. The top right is a POV-Ray rendering shows the quadrupole trapping region where particles are confined with respect to the electrode poles, and the bottom right shows the normalized inhomogeneous harmonic electric fields (IHF) of the quadrupole electrode device which shows a distinct inhomogeneous electric fields (IF) minima at the center of the electrode gap. The color bar scales linearly from $E/E_0 = 0$ to $E/E_0 = 3$. The use of DCPM techniques for these non-canonical topologies represents a significant achievement in the ability to construct multi-scale models of the particle systems and translate these into the macroscopic performance of devices.

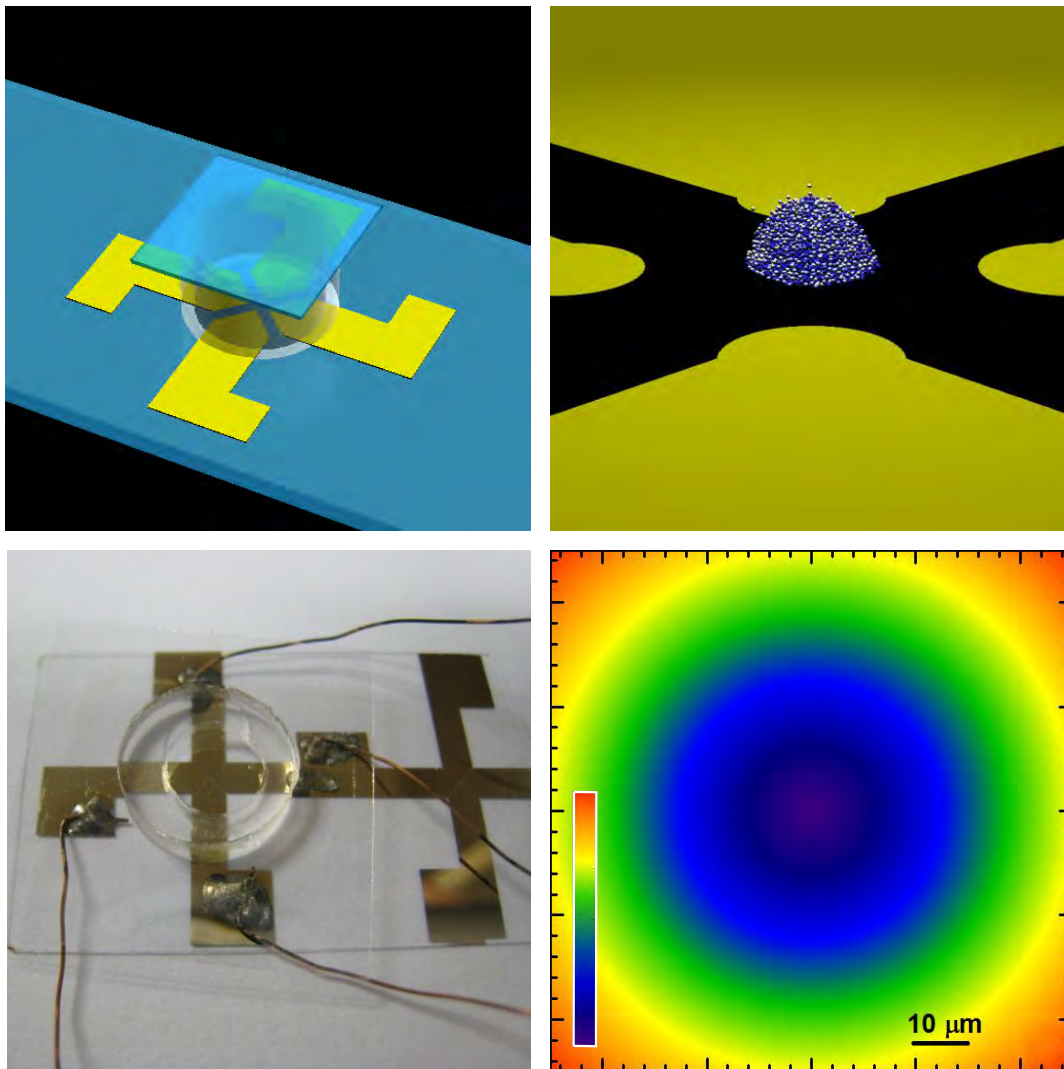


Fig. 5 – Quadrupole electrode geometries (left) used to generate for inhomogeneous fields (bottom right) and inhomogeneous harmonic electric fields for particle trapping (top right).

2. Measurement and Characterization of Electromagnetic Properties at High Frequencies: Characterize the intrinsic electromagnetic properties of colloidal-based materials and relate them to the global performance of an ETCM-based reconfigurable antenna.

- i. Determine practical limitations, realizable tuning ranges of electromagnetically functional colloidal suspensions, and the effects of in situ mixing and changing concentration, particle size, and media*

Numerous efforts were made using commercially-available BaSrTiO_3 colloidal material (from TPL, Inc.), but the high viscosities that resulted from the desired dielectric increases from mixing these spherical shapes into a non-ionic fluid were deemed impractical for an antenna application. The synthesis of high aspect ratio BaTiO_3 nanowires was investigated in lieu of commercially-available nanoparticles with a high aspect ratio and high dielectric constant (for highly tunable dielectric dispersion). A molten salt method was chosen to synthesis high aspect ratio BaTiO_3 nanowires; the mechanism of molten salt method is similar to that of the solid-state reaction, but the salt plays an important role from intervening in the formation reaction. This method is an easy and low-cost method but have other advantages like chemical methods, such as relative low temperature and high purity. Scanning electron microscope (SEM), X-ray diffraction (XRD), and electron backscatter diffraction (EDS) Mapping were used to characterize the prepared products of BaTiO_3 nanowires. The images indicated that suitable cleaning processes, including centrifuge and water wash, played an important role in purifying the sample. High purity samples could be obtained by centrifuging 20 times and water washing 50 times. During examination of the materials it was found that the synthesis process of BaTiO_3 nanowires using quartz crucible leads to the development of the second-phase product BTS (in addition to the BaTiO_3 nanowires). A zirconia crucible was used to avoid producing BTS, and single crystalline, high purity and high aspect ratio BaTiO_3 nanowires were successfully synthesized. Fig. 6 shows several different particle morphologies that could be achieved in using this method.

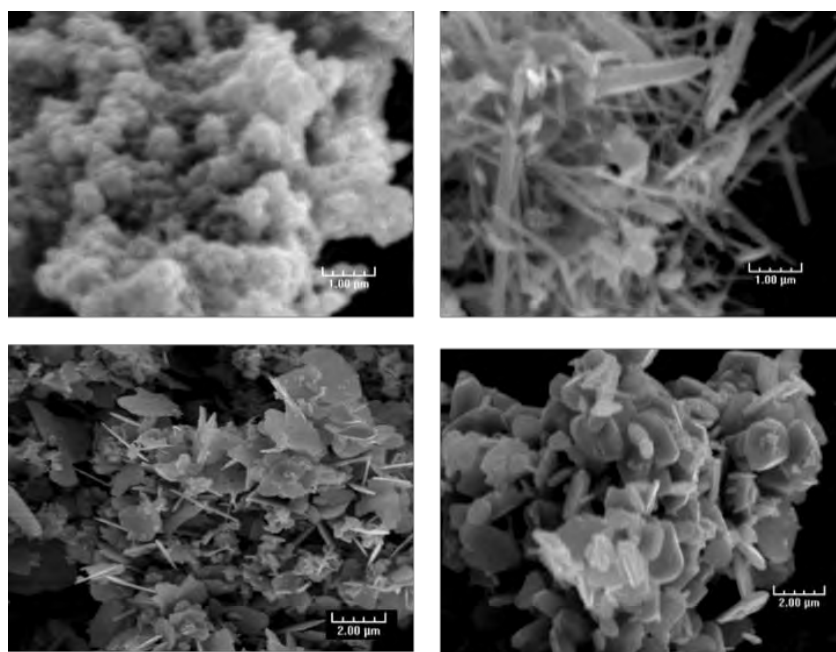


Fig. 6 – Examples of particle morphologies which can be achieved through adjusting the processing steps of the molten salt method for the creation of high aspect ratio BTO nanoparticles.

Fig. 7 shows a summary of key experiments on the synthesis process and the resulting impact on the particle morphology. The BTO nanowires were chosen from these as a candidate for EM mediated alignment because of their strong contributions to the dielectric mixing (according to predictive modeling by the Maxwell-Garnett mixing formula). The nanowires had diameters ranging from 100 nm to 300 nm, and their lengths ranged from 1.5 μm to 5 μm . These high aspect ratio BaTiO_3 nanowires using molten salt method exhibited a very high sensitivity to annealing temperature, annealing time, and the choice of TiO_2 precursor. Single crystal, high purity, and high aspect ratio BaTiO_3 nanowires could therefore only be synthesized only under certain conditions: using TiO_2 anatase nanospheres with diameter 15 nm, choosing annealing time 3.5 hours, and annealing temperature 820 $^\circ\text{C}$. Short aspect ratio BaTiO_3 nanowires were attained if using TiO_2 rutile nanoparticles were used as the precursors. The nanocubes would be synthesized instead of nanowires if the annealing temperature was not high enough or the annealing time not long enough. Interesting particle morphologies, termed “nanoflowers,” were produced if the annealing temperature was more than 950 $^\circ\text{C}$. This illustrated that successful production of BaTiO_3 nanowires depended on processing time, processing temperature and the crystalline phase. Fig. 8 shows a matrix of preliminary experiments to examine the alignment of BTO nanowire particles. The results indicate that the particles can be aligned accordingly in an electric field.









Reaction materials (TiO_2)	Pre-heating (Yes/No)	Processing time (hour)	Processing temperature ($^\circ\text{C}$)	Composition (according to XRD pattern)	Shape (Aspect ratio)	SEM
Antanase, 15 nm	Yes	3.5	820	BaTiO_3	Nanowires (around 2-10)	
Antanase, 15 nm	No	3.5	750	BaTiO_3 , BaTi_2O_5	Nanocubes (around 1)	
Antanase, 15 nm	No	3.5	950	BaTiO_3 , $\text{Ba}_4\text{Ti}_{13}\text{O}_{30}$	Nanoflowers (plates)	
Antanase, 15 nm	No	2.5	820	BaTiO_3	Nanocubes and Nanowires	
Antanase, 15 nm	No	4.5	820	BaTiO_3	Nanocubes and Nanowires	
Rutile, 10*40 nm	No	3.5	820	BaTiO_3 , BaTi_2O_5	Nanowires (around 2-5)	
Rutile, 50 nm	No	3.5	820	BaTiO_3 , BaTi_2O_5	Nanowires (around 2-5)	
Antanase, 15 nm	No	3.5	820	BaTiO_3	Nanowires (around 12-15)	

Fig. 7 – A summary of molten salt experiments to determine the impact of processing steps on the particle morphology and material characteristics.

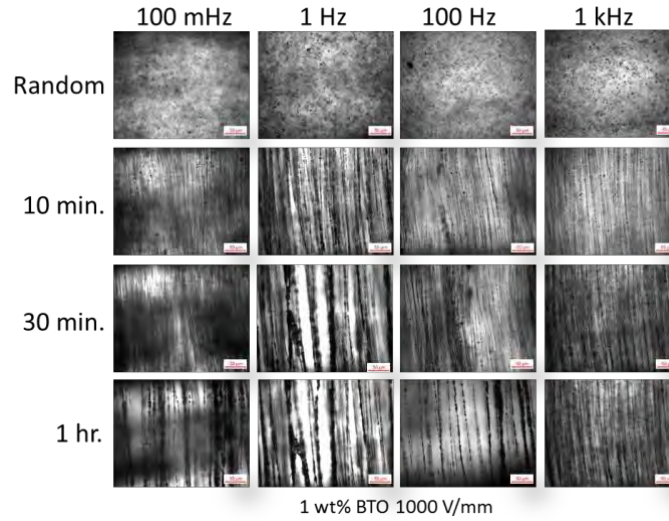


Fig. 8 – Matrix of experiments on the alignment of nanowire BTO in an electric field.

The impact of electric field parameters on their alignment in a dielectric medium (oil) using planar electrodes and the synthesized nanowires shown (Fig. 6) was investigated with more detail. This resides at the core of our microfluidic approach: to exploit and tune transport properties of high permittivity colloidal assembly to controllably adjust their electromagnetic response at the macroscale through electric field directed assembly. An in-depth electric field-driven processing of the BTO nanowires in oil was conducted for this and relevant results of the obtained microstructures are summarized in Fig. 9 for a range of times, electric field frequencies and magnitudes. It was found that a combination of low frequency (10 Hz and less) at low voltages (100V) for a duration higher than 10 minutes results in rotation and chaining of the nanowires. The PIs have demonstrated that chainin, not just rotation, results in the highest impact on the electrical properties.

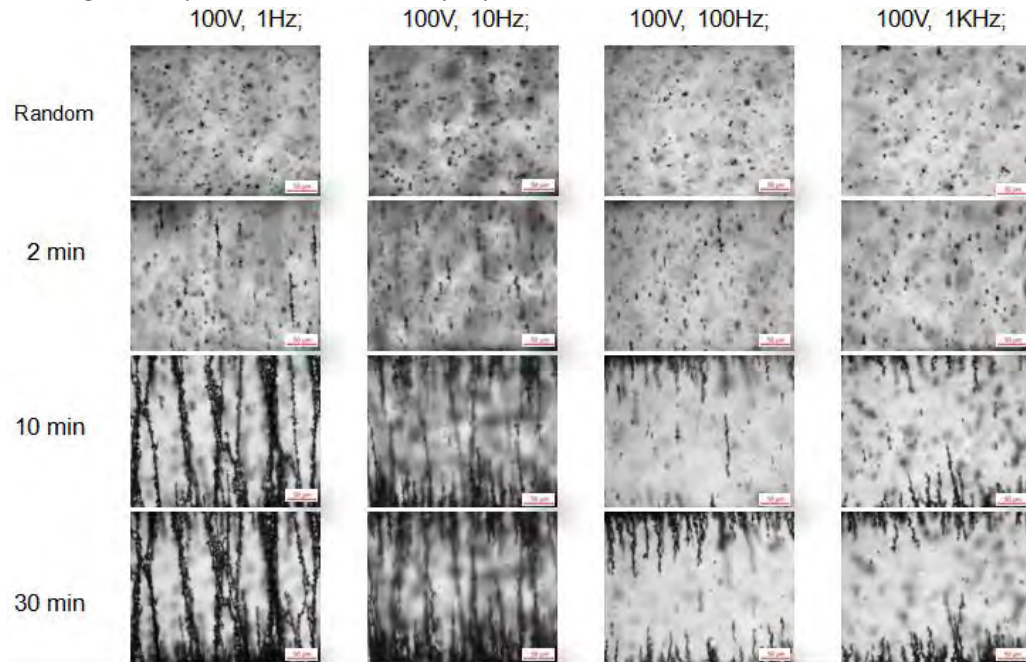


Fig. 9 – Electric field-driven processing of the BTO nanowires in oil.

The capacitance increase (as compared to the capacitance of air for the planar electrode geometry) was measured for these samples to quantify the impact of the aligned microstructures on the effective dielectric behavior. This is shown in Fig. 10 for the randomly dispersed BTO nanowires in oil and the aligned BTO using 100 V and three different alignment frequencies (10 mHz, 10 Hz, and 1 KHz). The behavior mirrors the microstructure shown in the previous figure. At the lower frequencies, (10 mHz and 10 Hz), chains of BTO nanowires bridge across the electrodes, resulting in the biggest impact to the properties. At higher alignment frequencies, such as at 1 KHz, although the BTO rotate in the direction of electric field; the chains that form are shorter and the impact on properties is lower. These results are for low-frequency alignment frequencies but this data (and other sets taken during this project) provides significant insight into the behavior of these particles and a link between the synthesis of particles and the ability to influence their alignment in an electric field.

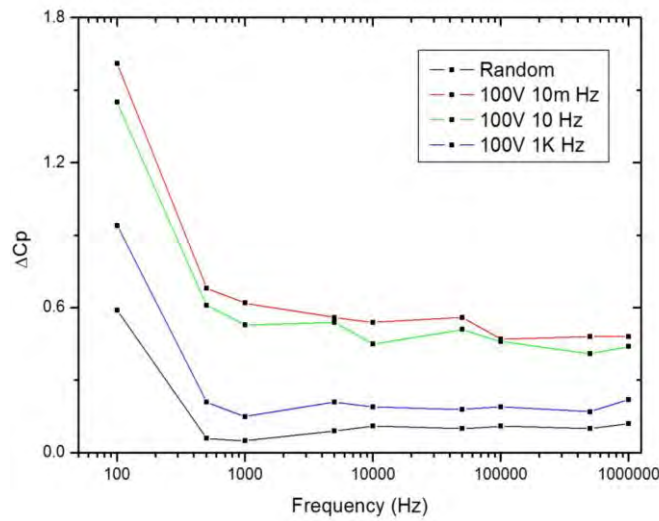


Fig. 10 – Capacitance measurements from electric field-driven processing of the BTO nanowires in oil.

ii. Develop robust test fixtures and reliable measurement techniques to evaluate the electromagnetic properties at high frequencies of static and dynamic pressure and electric field-driven systems

The next step in understanding the device-level functionality of an enabling mechanism based on colloidal dispersions (homogeneous mixed, fluidic-driven, colloidal material system) is accurately characterizing their effective constitutive properties (permittivity ϵ_{eff} , permeability μ_{eff} , and conductivity σ). Mixing rules based on the volume fraction of colloidal material in the liquid provide significant insight into this process, but the accurate measurement and validation of these dynamic material systems is a key step to understanding their role. This is especially true once the overall device complexity increases and compositions of different materials and/or fluids are used so a fluid measurement cell based on the coaxial transmission line topology has been constructed in this project to accurately characterize these constitutive parameters. A static version of this device without fluid inlets and outlets has been fabricated and used, where the RF connectors are removed for each experiment so the chamber can be cleaned, filled with a new dispersion, and sealed again using the RF connectors. A dynamic version with fluid inlets and outlets has also been constructed so in situ experiments can be performed. A CAD model

of the cross-section of this coaxial measurement device can be seen in Fig. 11 (right). It provides a very accurate measurement of the dispersion's material properties, which can be extracted using its measured S -parameters (related to impedances). The basic measurement set-up for this has been included on the right side of Fig. 11.

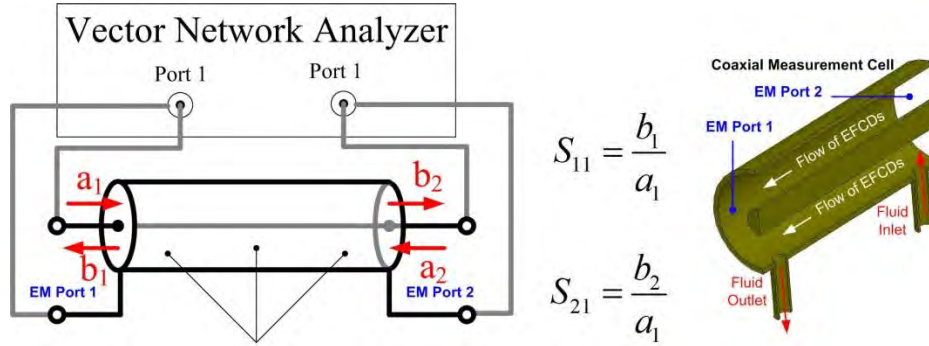


Fig. 11 – Coaxial measurement cell for the characterization of EFCD (fluid-based) materials.

The aforementioned fluidic measurement system provided measurements of fluidic nanoparticle dispersions, and allowed them to flow through the cell during the high frequency characterization process so mixing and other activities could be performed. It provided a good estimate of material properties, but many of the materials examined in this project were set into an epoxy and cured to a solid composite so microscopy could be used to evaluate the alignment and particle morphology. A “free-space” material measurement system was constructed for this project to measure these composites (and other planar coupons of materials). The left side of Fig. 12 shows a low-cost prototype of this measurement system, the middle of Fig. 12 shows the functional components of this (two X-band horn antennas) along with the material under test (MUT), and the right side of Fig. 12 shows the analytical model of the measurement which is used to derive closed-form expressions. This model can then be used to extract the dielectric permittivity and magnetic permeability of the MUT (a transmission line model of this is also shown in the bottom-right). This system was automated so repeatable measurements and calibrations could be performed.

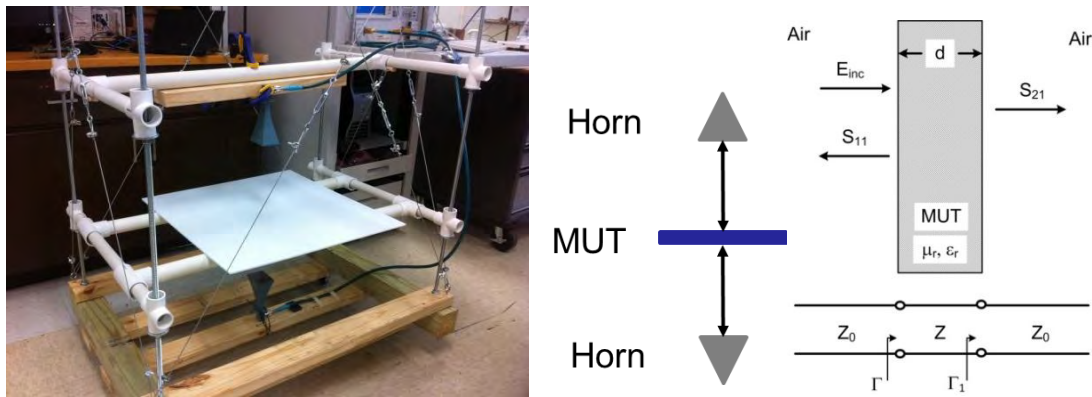


Fig. 12 – (Left) Free-space material measurement system, (middle) essential components of the measurement, and (right) the mathematical model of the test used to extract the material parameters.

The automated free-space measurement system relies on an Agilent E8361C PNA to measure the S_{21} parameter of the measurement apparatus and material sample (this is similar to one of the measurements used in the coaxial cell). The network analyzer is controlled over a TCP/IP network by a LabVIEW virtual instrument (VI). The VI uses the Virtual Instrumentation Software Architecture (VISA) to send Standard Commands for Programmable Instruments (SCPI) instructions to the network analyzer. These are used to calibrate the system, take the required measurements, and save the measured data to an unformatted Citifile on a network drive hosted by the automation computer. In addition to taking averaged measurements of the S_{21} parameter, the VI can be configured to command the network analyzer to apply a range of time-domain gating (or windowing) to the measured signal to reduce the effect of diffraction and reflection of the test signal around the sample. The VI then commands a MATLAB script to import the data from the Citifile, shift the reference plane of the measured data out from the center of the system to the top and bottom of the sample, and use Mueller's iterative method to solve the S_{21} equation for the relative permittivity. The MATLAB script outputs a JPEG image containing plots of the measured S_{21} parameters, their reference-shifted counterparts, and the calculated permittivity and loss tangent across the range of frequencies measured. Fig. 12 shows the calibration steps (screen-shots of the VNA from left to right on top, then left to right on bottom) which are used to remove the undesirable reflection from cables and other undesirable artifacts of the measurement system. This process involves the transform from frequency domain to time domain in order to set the correct reference plane and gat out the undesirable reflections.

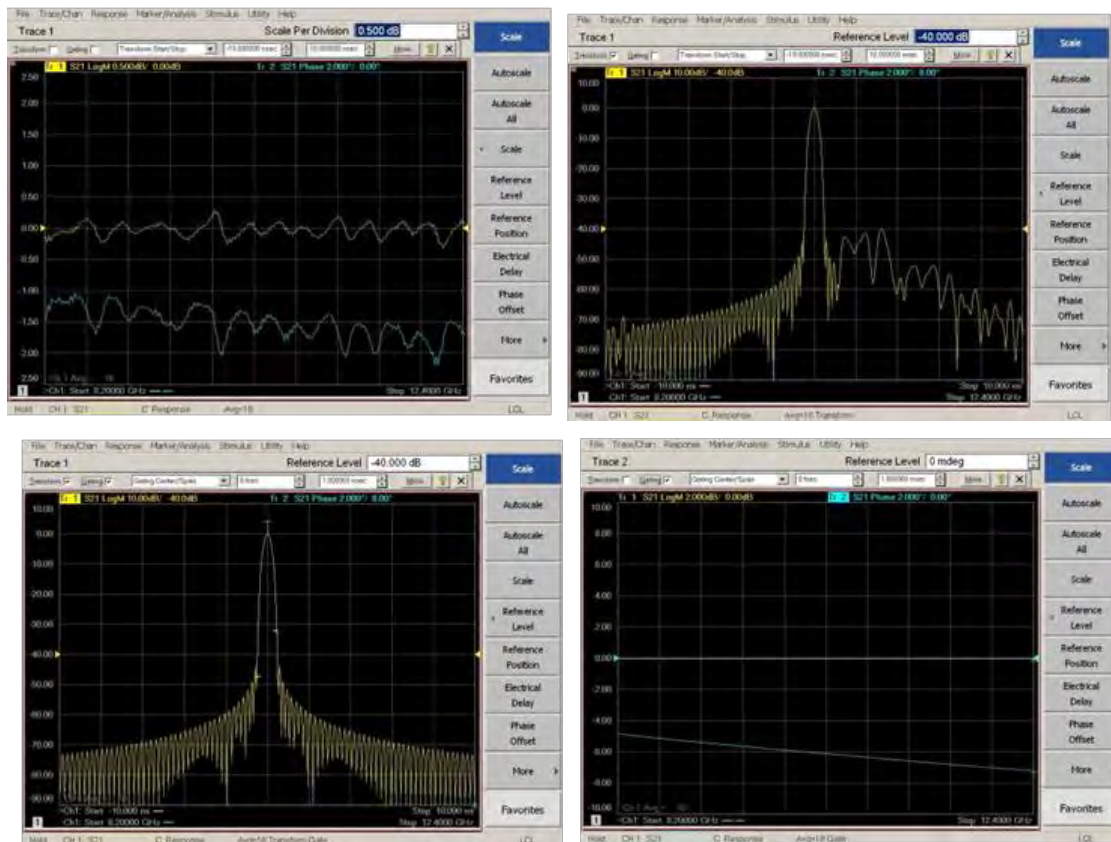


Fig. 12 – Calibration process used to remove undesired reflections from cables and other artifacts of the measurement system; uncalibrated measurement in frequency domain (top left), uncalibrated measurement in time domain (upper right), time-gated measurement in time domain (bottom left), and final calibrated measurement in frequency domain (bottom right).

Fig. 13 shows the LabView VI which was used to automate the measurement process. This provided complete control and immediate post-processing of the measured results. Two sets of microwave horns were used in this project to characterize composite materials; X-band (from 8 GHz to 12 GHz) and Ka-band (from 26.5 GHz to 40 GHz). Fig. 14 shows the measured results for plexiglass in X-band (right) and Ka-band (left); this is a well-known material that can be used to evaluate the performance of the system. The results are in good agreement for both bands; this system has been used for other materials and can be applied to materials developed in future projects.

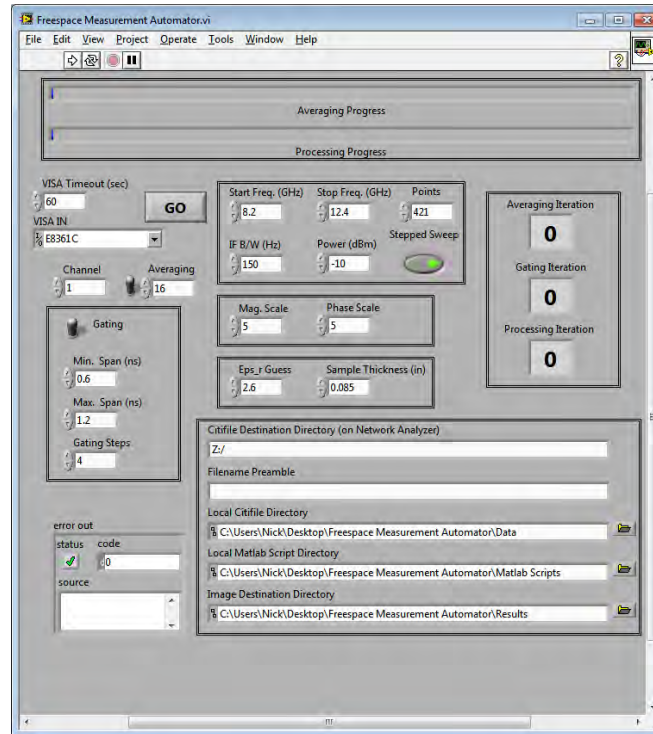


Fig. 13 – LabView GUI used to automate the materials measurement process.

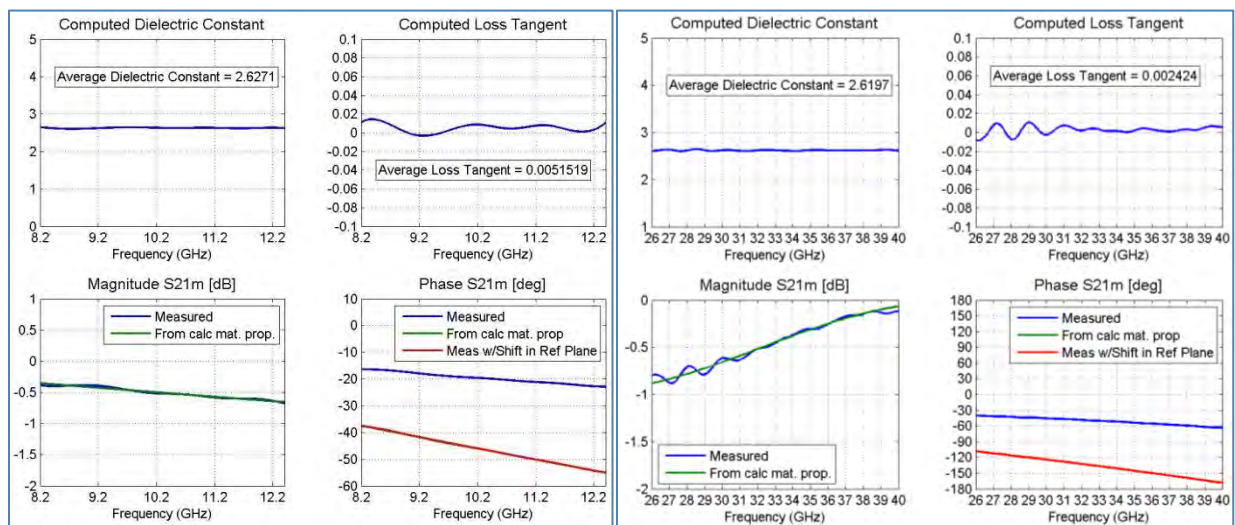


Fig. 14 – X-band (left) and Ka-Band (right) characterization of plexiglass using the automated free-space material measurement system.

iii. Relate the performance of antenna parameters to the fundamental materials properties through multi-scale equivalent circuit representation and modeling

One of the key objectives for this project is to develop a demonstration vehicle which can provide linkage between length scales – from nanoscale particle behavior to microfluidic flow to macro-scale antenna performance (system behavior). Fig. 15 shows the diagram of the polarization reconfigurable antenna that has been developed as a demonstration vehicle for this purpose, and Table I provides the dimensions shown in this figure. The antenna is composed of two narrow and orthogonal microstrip patch antennas that behave as printed dipoles. The antenna is fabricated on a Duroid® 5880 substrate (a low-loss microwave laminate formed from Teflon and woven fiberglass with a relative permittivity $\epsilon_r = 2.2$ and height $h = 1.57$ mm. This height is $0.013 \lambda_0$ at the design frequency $f_0 = 2.442$ GHz, which is the center of the Industrial-Scientific-Medical (ISM) band. The choice of this frequency band reflects the goal of being able to transition these technologies, and to coordinate the design these systems so they can operate within range of frequencies that are amenable to Air Force applications.

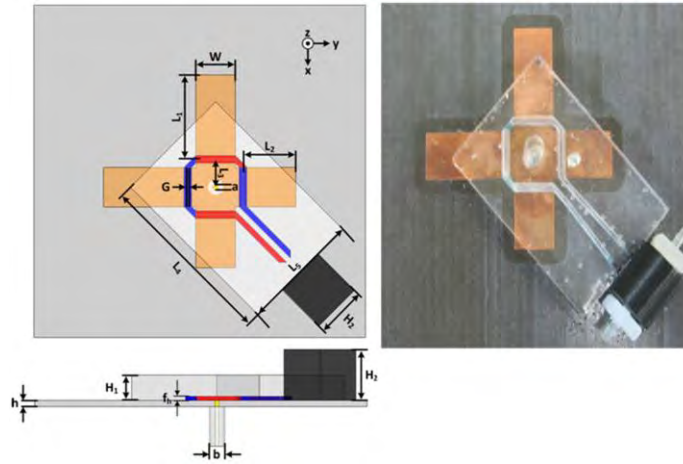


Fig. 14 – Polarization reconfigurable antenna using fluidic dispersions (including custom fluidic networks and connectors); CAD model on left and fabricated structure on right.

Table I. Dimensions of the crossed dipole antenna enabled by colloidal dispersions.

H_1	H_2	L_4	L_5	f_h	W	G	a	b	h	L_1	L_2	L_3
6.4	12.9	45.7	30.5	1.0	10	0.3	1.23	4.1	1.57	21.2	13.2	6.85

Radio frequency (RF) excitation of the antenna is provided at the intersection of the two patch antenna structures using a Sub-Miniature Type-A (SMA) coaxial probe connector. The four symmetric gaps of width $G = 0.3$ mm are placed at the intersection of the two radiators enable the structure to alternate polarizations. Reconfiguration is accomplished by changing the effective medium properties of the fluidic-based materials that placed across these gaps – this changes the capacitance and effectively turns the two dipoles ‘on’ or ‘off.’ A microfluidic network was designed and tested using Inventor, Solidworks, and COMSOL. Sylgard (PDMS) with $\epsilon_r = 2.66$ and $\tan\delta = 0.03$ was selected as the material for the microfluidic cap. An adapter, 12.9 mm square, interfaces with the PDMS microfluidic cap and pumping systems. The first mechanism alternates between high and low permittivity dispersions or fluids (shown as red and blue in Fig. 14)

Fig. 15 shows the measured input impedance and VSWR for the fluid displacement mechanisms. The experiment was conducted by periodically alternating immiscible fluids so they properly load the four gaps – a petroleum distillate oil ($\epsilon_r = 2.1$) and deionized water ($\epsilon_r \sim 80$). Fig. 15 shows the measured frequency behavior of the antenna for both configurations (e.g., rotating the red and blue fluids by 90 degrees around the gaps) at 2.74 GHz and both x and y linear polarizations agree. The water-tight seal had problems during the experiment causing water to leak into an adjacent channel section. The water forced the oil to move into another channel section leaving three consecutive sections containing water. The added impedance from the additional antenna segment reduced the impedance match. Because the water was seeping into another channel, part of one gap was not completely covered. This caused a reduction in coupling changing the antenna's length. Nonetheless, the fabricated antenna successfully demonstrated the concepts of using a fluidic varactor to switch polarizations.

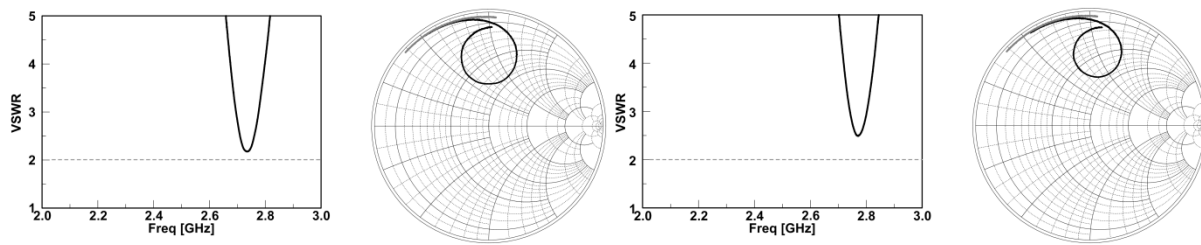


Fig. 15 – Measured VSWR and impedance of the antenna (x-polarized on the left and y-polarized on the right).

A second design (shown in Fig. 16) was also created to improve the performance of the pressure-driven network and exploit the electrokinetic behavior of the particles in addition to the fluidic displacement of the dispersions. An applied electric for field biasing is delivered to each arm through the bias networks; these are the four thin quarter-wavelength lines terminated in a shorting capacitor and bias resistor. This are able to be used for alter particle alignment via dielectrophoresis, which was not attempted in this project due to concerns over possible damage or misuse of measurement equipment, but they are have been simulated using the effective medium properties derived from other work in this project and the antenna performs well. The new fluidic system was tested and it worked very well.

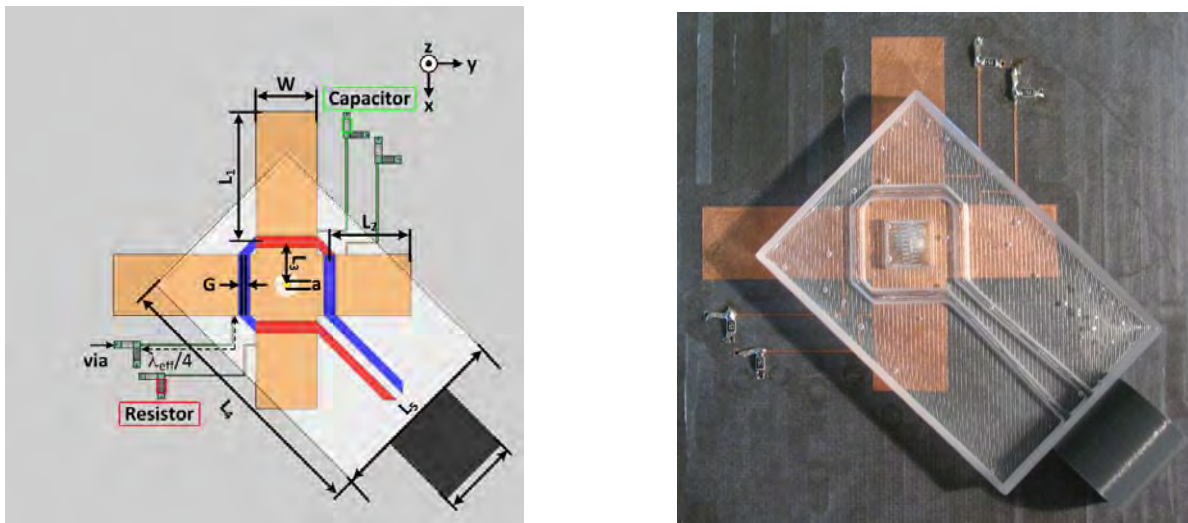


Fig. 16 – Second design of the polarization reconfigurable antenna; the addition of four bias networks will provide a means to bias the arms and exploit the electrokinetic properties of the dispersion.

Figs. 17-19 show the measured, simulated, and analytically-derived (using the transmission line model discussed in the next section) performance of the antenna for three reconfigurable states of the antenna. Each state corresponds to the fluid displacement across the gaps; the off-state with no fluid across the gaps (Fig. 17), the first “on” state (Fig. 18) with water in gaps 2 and 3 (dyed blue) and air in gaps 1 and 4, and the second the “on” state (Fig. 19) with water in gaps 1 and 4 (dyed blue) and air in gaps 2 and 3. The results in these figures include the input impedance (shown on Smith Charts), the voltage standing wave ratio (VSWR), and radiation patterns in the two primary elevation cut-planes (xz- and yz-plane). The fabricated antenna successfully demonstrated the ability to implement a “fluidic varactor” to switch polarizations.

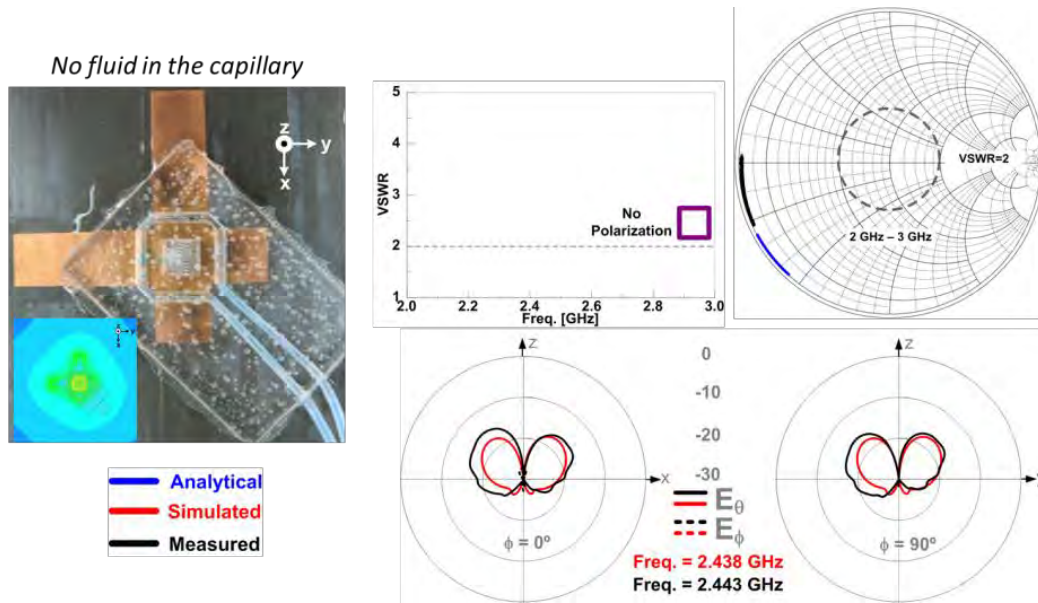


Fig. 17 – Fabricated antenna and measured parameters for the reconfigurable antenna in an “off” state.

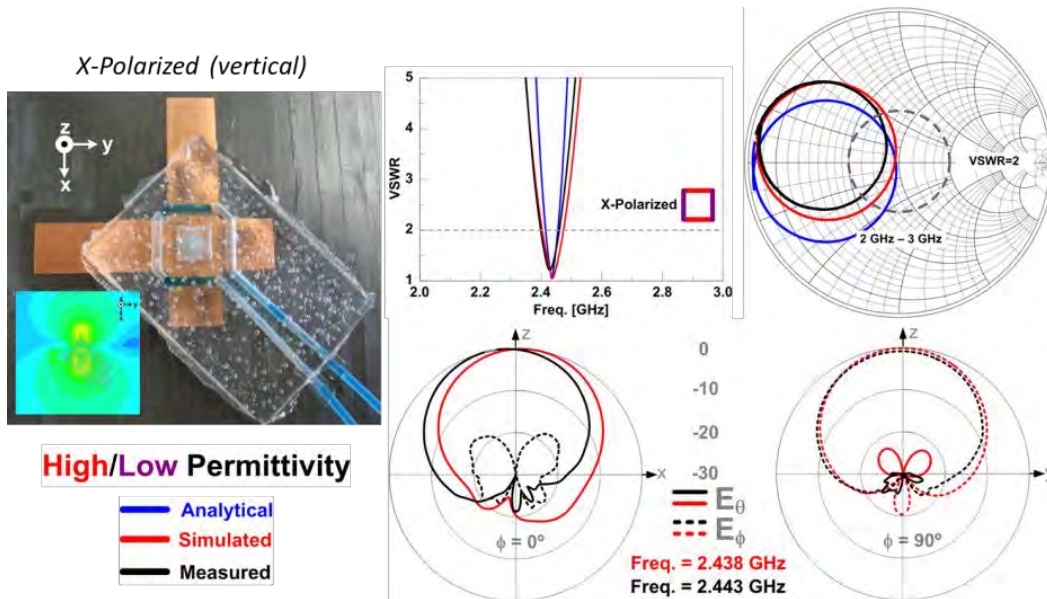


Fig. 18 – Fabricated antenna and measured parameters for the reconfigurable antenna in an “on” state which is polarized along the xz-axis.

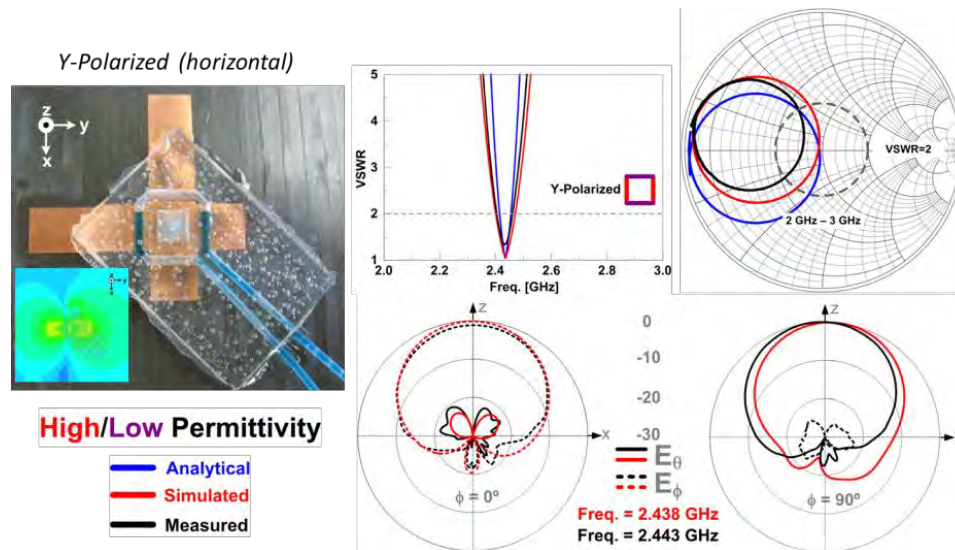


Fig. 19 – Fabricated antenna and measured parameters for the reconfigurable antenna in an “on” state which is polarized along the yz-axis.

3. **Multiscale modeling and simulation of EM performance of colloidal-based materials structures (ETMCs) using a multi-scale and physics based framework. We will develop modeling methodologies for optimization of the integrated, multifunctional colloidal-based materials and devices by first focusing on understanding the mechanisms of colloidal assembly and second on predicting the resulting effective properties of the assembled structures**
 - i. Develop a hierarchical multi-scale modeling methodology for the extraction of macroscopic electrical resistivity, permittivity and magnetic permeability tensors of the electromagnetically tunable colloidal material systems (ETCMs) under different patterning configurations

The COMSOL finite element software was used for numerical simulation of multi-physics and multi-scale models so it was first verified against the experiments of Bahukudumbi *et al.* from 2007 (the PI’s preliminary work for this project) before using COMSOL to predict effective properties of dispersions and other systems. These experiments consisted of two parallel planar electrodes separated by a distance of 30 μm (shown on the left in Fig. 20). A voltage difference of 2.5V was applied to the electrodes at frequencies of 10 Hz, 1 kHz and 100 kHz. No free charge is present outside of the double layer on the electrodes. A 3x3 array of gold particles (shown in the middle of Fig. 20) modeled as circles were centered successively at locations $n = 1, 2$ and 3 with $(x_n, y_n) = (1.2, 3), (40, 3),$ and $(90, 3)$, respectively (dimensions in μm). The electric and fluid forces were obtained by integrating the Maxwell and Cauchy stress tensors on the particle surfaces. These electric and fluid forces were summed to yield the total force on the center particle; these are tabulated in Table 2. The Fluid streamlines and electric potential (colors) are depicted on the right of Fig. 20. The results are in general agreement with the experiments of Bahukudumbi *et al.* (2007) and the results support the conclusions in that work. Specifically, the electric and fluid forces are negligible at 10 Hz; this is a low-frequency regime that is dominated by electrophoresis. At 1 kHz, the total force tends to push the center particle out of the gap to the outer edges of the electrodes. At 100 kHz, the total force tends to push the center particle to the inner edge of the electrodes. These results are also summarized graphically in Fig. 21.

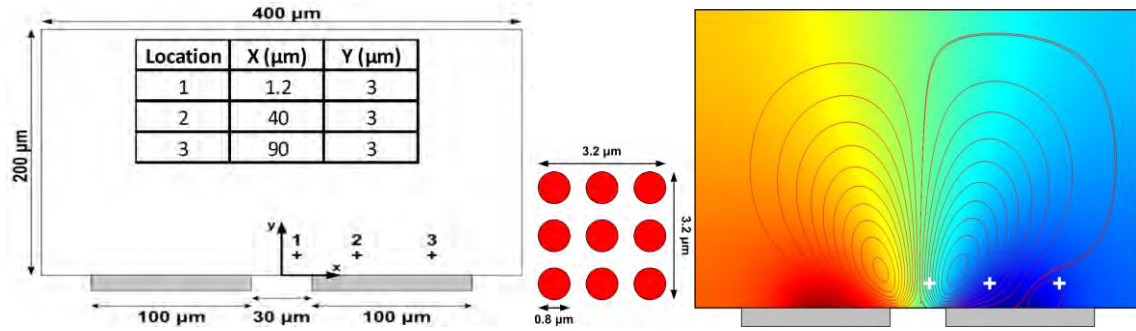


Fig. 20 – Domain of AC Dielectrophoretic simulation (left) and 3x3 array of gold particles (middle), and fluid streamlines with colored-mapped contours of electric potential (right).

Table 2 – Total force on the center particle.

Location	Freq (Hz)	Ftotalx (N/m)	Ftotaly (N/m)
1	10	1.36E-11	-3.16E-11
	1.00E+03	3.85E-08	-8.85E-08
	1.00E+05	1.26E-08	-1.46E-08
2	10	3.94E-10	7.48E-11
	1.00E+03	9.56E-07	2.20E-07
	1.00E+05	3.54E-09	-6.73E-09
3	10	3.58E-11	2.85E-11
	1.00E+03	4.51E-08	5.75E-08
	1.00E+05	-1.33E-10	-2.34E-09

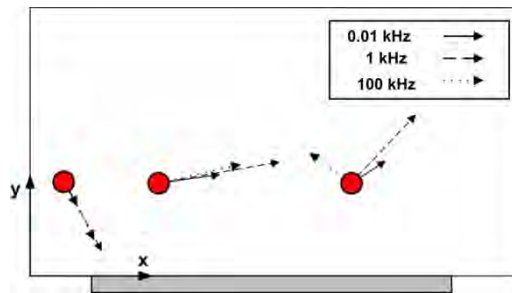


Fig. 21 Calculated forces on a single particle at different frequencies (only the single electrode on the right is shown).

A significant amount of work has also been performed in developing a framework to analyze the effective medium properties of the dispersion (in both random and microstructured states). Classical mixing rules are beneficial since they can benchmark the process for canonical particle geometries (spheres, etc.), but they have limitations that make computer modeling preferable under certain circumstances when aspect ratio and geometry are non-uniform. For example, mixing rules such as the Maxwell Garnett rule are less valid at high volume fractions due to their negligence of inter-particle effects. As some of the mixtures used in this study have relatively high volume fractions (>30%), computer modeling can be used for higher accuracy over classical mixing rules. These effective properties simulations were performed in a three step process. First, Matlab was used to generate a random, periodic distribution of spherical particles. Next, this periodic distribution was output to COMSOL, a commercial multi-physics finite element program. Finally, COMSOL was used to calculate the effective permittivity of the medium. In this study, effective property simulations of barium strontium titanate (BSTO) in a silicon oil medium were conducted for volume fractions ranging from 10%-40% in 10% increments. A MATLAB program was created to generate the random, periodic distribution of

particles within a specified volume fraction. The input variables for the routine are particle radius, volume fraction, and number of particles. The program then generates a random distribution based on the given parameters.

Due to the nature of nanoparticle suspensions, the distribution of BSTO particles within the oil is inherently random. In order to reflect the randomness of the mixture in the simulation, the MATLAB algorithm incorporated a random number generator to distribute the spheres in a specified volume. The random number generator uses a brute-force technique to insert spheres into the volume. Consequently, the algorithm tends to be less effective with high numbers of spheres or volume fractions in excess of 50%. The program also used a brute-force method to ensure periodicity. In a periodic distribution, all inclusions can be represented by a representative volume element (RVE). The RVE chosen for this case is a cube with spherical inclusions. For the RVE to be periodic, each of the spheres that intersect one or more faces of the RVE must be replicated on the opposite face. The periodic conditions allow the RVE to represent a much larger system than itself, in such a way that the capillary system domain can be represented by the much smaller RVE domain. RVE's for volume fractions of 10%, 20%, 30%, and 40% were created. These are shown in Fig. 22.

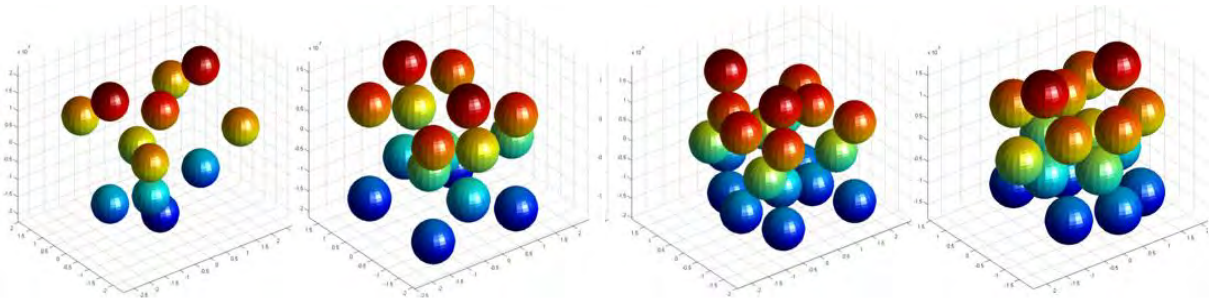


Fig. 22 – Representative volume element (RVE) for a cube with spherical inclusions; this framework enables the examination of mixing formula and the extension of their predictive capabilities to more exotic particles.

The particle geometry is then imported into COMSOL, where the RVE is created. This is done by grouping all of the imported objects and then discarding all spheres or portions of spheres outside of the RVE cube. Then, subdomain and boundary conditions are applied to the RVE. The steps in the analysis of a single RVE are illustrated in Fig. 23 to demonstrate the modeling process. All spheres were assigned a relative dielectric constant $\epsilon_r = 1000$ and the medium outside the spheres was assigned $\epsilon_r = 2.1$; these values are in accordance with the real/predicted values of the dielectric constant for the BSTO and the oil, respectively. Periodic boundary conditions were then applied to the RVE so that COMSOL could analyze the system as a periodic element.

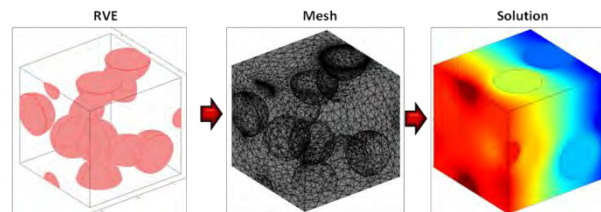


Fig. 23. Modeling process for representative volume element (RVE) using a cube with spherical inclusions.

The system is then meshed into thousands of elements so that the problem can be solved by finite element analysis. The solution yields the values of the electric displacement in the x, y, and z directions for an element of specified volume fraction and with a voltage gradient in a single direction. After repeating this process for voltage gradients in the two remaining Cartesian directions, the entire effective permittivity matrix for the element was determined. Each of the four volume fractions of 10%, 20%, 30%, and 40% were simulated for voltage gradients in the x, y and z axes. This entire process was then repeated two more times in order to create an average of the results. In total, 36 separate simulations were performed, resulting in the data shown in Fig. 24. In addition to the effective permittivity for the x (11), y (22), and z (33) directions in the element, the yellow line signifies the average of the effective permittivity over all directions. Also, the Maxwell Garnett mixing rule and percent error between the isotropic average and Maxwell Garnett mixing rule are plotted. We anticipate the convergence of these results with greater sampling (e.g., if a statistically more comprehensive examination was examined). This process can now be used to examine more exotic particle geometries.

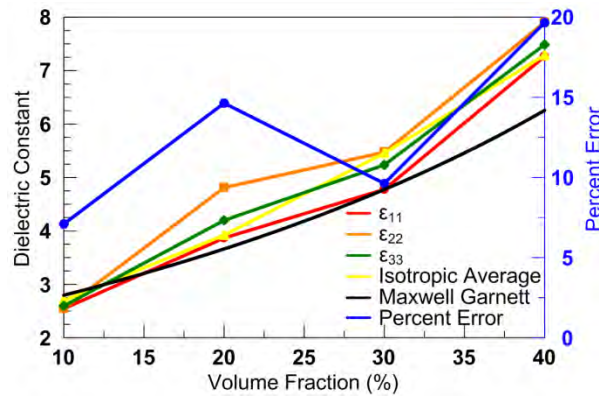


Fig. 24 – Results from modeling process using the representative volume element (RVE) as a cube with spherical inclusions.

ii. Use effective electromagnetic properties for the electromagnetic analysis of integrated colloidal suspension components

A transmission line model of the previously-discussed polarization reconfigurable antenna has been developed to analytically predict the impedance of the antenna across a reasonably large bandwidth. It also acts as an analysis tool for studying the impact of different material systems and provides a truly multi-scale representation of the work in this project. Fig. 25 shows the antenna model developed for this, in which the four ‘black-box’ gaps correspond to those seen in Fig. 16 (the “Radiating Edge” includes radiation resistance and edge capacitance). The gaps in this model include information about composition and concentration of nanoparticles in the fluidic the dispersions which flow across them.

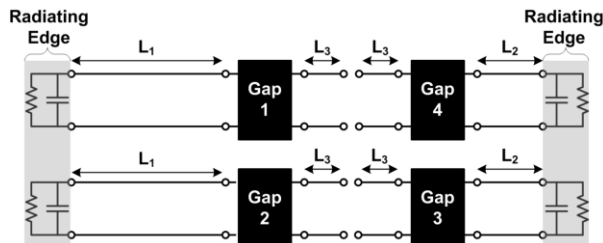


Fig. 25 – Transmission line model of the antenna shown in Fig. 1.

A physical cross-section of the gaps and their circuit model is shown on the left side of Fig. 26; a conformal mapping model of the gap (right side of Fig. 26) has been developed to provide a physically intuitive link between the high frequency performance-governing electromagnetic field distribution across the gap and the impact of particle composition and concentration in the capacitive contributions from the gap topology. The perfect electrical conductor (PEC) shown on this model is a result of symmetry, and makes the conformal mapping analysis possible; it bisects the equivalent circuit model (center of the gap). This represents a significant effort in the development of a multi-scale model since the full analysis of particles in the gap is computationally expensive, time consuming, and contains length scales which cause numerical instabilities with many numerical methods (finite element, etc.).

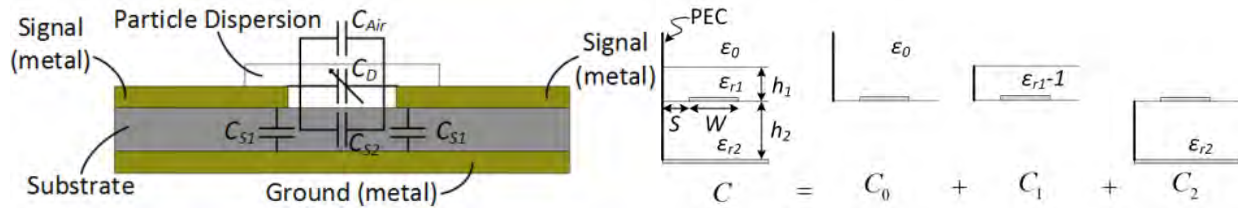


Fig. 26 – (Right) Cross-section and (left) equivalent circuit model of the gaps shown in Figs. 1 and 2.

The *COSMIX* (right side of Fig. 27) illustrates another example of our activities in this area that link macro-scale designs with analytical and numerical techniques that describe the effective electromagnetic properties; these enable the accurate electromagnetic analysis of integrated colloidal suspension components. The *COSMIX*'s equivalent circuit (embedded in the Smith chart shown on the left of Fig. 2) illustrates the similarity of this to the coaxial measurement device and shows how the volume fraction \mathcal{V} of colloidal material can impact the coaxial structure and its termination (every parameter of the device is linked to the volume fraction of colloidal material in the fluidic medium).

The CAD model shows the inlet and outlet for fluid flow down the length of the *COSMIX*. These can be modeled as circular waveguides connected in parallel at their location on the coaxial line, which has a characteristic impedance $Z_0(\mathcal{V})$ and complex propagation constant $\gamma(\mathcal{V})$. In this case all of the information on the particle distribution has been encapsulated within the description of $Z_0(\mathcal{V})$ and $\gamma(\mathcal{V})$. The field structure of the coaxial line and their orientation will excite a *TM*-mode. The inlet/outlet diameter t and effective material properties of the *EFCDs* are chosen so these delivery systems remain well below cut-off so no guided modes develop in these structures. As such, they can be modeled as parallel loads with values given by their reactive impedance in cut-off (e.g., very large capacitors in parallel a coaxial transmission line) – these will have a negligible contribution within the context of operation consider here. The experiment, analytical model (using design equations), and simulations use: $L = 10$, $a = 2.05$, $b = 0.615$, $d = 0.15$ (in millimeters), and *EFCDs* with $\mathcal{V} = 0\%$ and 50% using non-magnetic <100 nm polydispersed colloidal *BSTO* ($\epsilon_{p2} \sim 800$, $\sigma_2 \sim 10^{-3}$) in silicon oil ($\epsilon_{r1} \sim 2.4$, $\sigma_1 \sim 10^{-8}$). Measured, modeled, and simulated results for this structure agree very well, and demonstrate how these techniques (perturbation, variational, etc.) will be developed in this project and advanced to analyze the increasingly complex structures and material systems we will investigate.

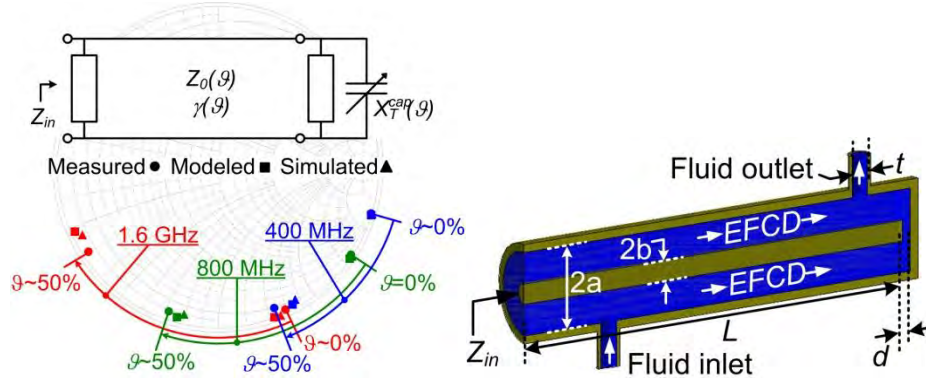


Fig. 26 – Measured, modeled, and simulated results (left) for the coaxial stub microfluidic impedance transformer (COSMIX) (right).

The phase-reconfigurable, microstrip patch reflect-array element (shown in Fig. 26) has also been used to investigate the performance of antenna parameters to the fundamental materials properties through multiscale equivalent circuit representation and modeling. These elements are often hindered by bias lines and other control structures if reactive-tuning or reconfiguration is desired to enable beam-steering, adaptive nulling, etc. in large arrays (adjusting the phase of nearby elements creates this functionality). The *COSMIX* provides a modular, circuit-like mechanism with a high tunability, low losses, and no need for biasing lines, etc. near the radiating fields of the antenna. The coaxial geometry is often used as a feed mechanism for driven elements so the pairing of the two is very straightforward.

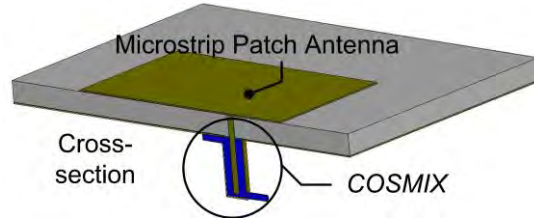


Fig. 26 – The phase-reconfigurable, microstrip patch reflect-array element

As an enabling mechanism, the *COSMIX* facilitated more than 360° of re-radiated phase shift (with minimal losses) by altering the composition of *EFCDs* and reactively loading the patch; it remained shielded below the ground plane so there are no parasitic effects from biasing or control lines to hinder the system-level performance. This simulation and experiment (results shown in Fig. 6) provides the first demonstration of an *EFCD*-based mechanism integrated into a reconfigurable antenna system.

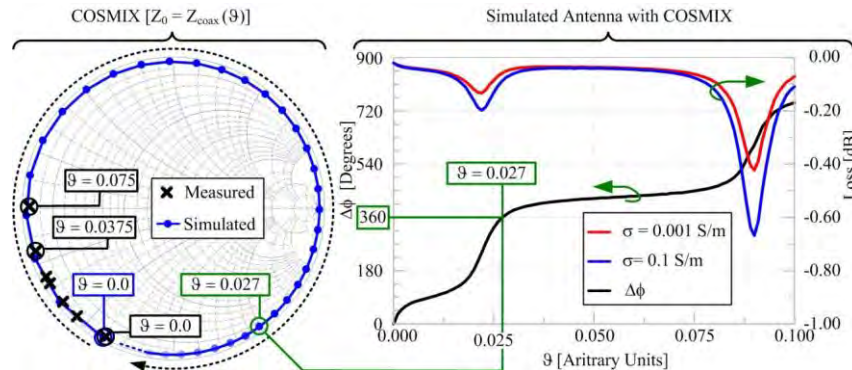


Fig. 26: The phase-reconfigurable, microstrip patch reflect-array element

4. Summary of Milestones and Accomplishments

In summary, this project has successfully integrated analytical and numerical/computational techniques into the multi-scale modeling of multi-physics systems. The primary focus has been on achieving a more complete understanding of fluidic dispersions based on colloidal materials in electromagnetic devices (with a particular emphasis on enabling reconfigurable antennas). The yearly accomplishments and milestones have been summarized for the performance period of this effort. These are:

i. Year 1 (JUN-2008 to JUL-2009)

- a.** Developed new methods and refined existing means to experimentally characterize the constitutive material properties (electrical permittivity, magnetic permeability, and electrical conductivity) of electromagnetically tunable fluids (ETFs)
- b.** Multi-physics modeling of these systems to link the fluidic forces, particle-level interactions, and electric field assisted spatial manipulation of particles
- c.** Examined the ability of these dynamic material systems in high frequency (up to GHz) devices as an enabling mechanism to achieve high performance in a multifunctional environment (structurally, electromagnetically, etc.)

ii. Year 2 (JUN-2009 to JUL-2010)

- a.** Development of a reconfigurable antenna demonstrate vehicle for fluidic and electrokinetic reconfiguration mechanisms
- b.** Characterization of the effective medium properties of colloidal dispersions as a function of frequency and particle composition
- c.** Synthesis and processing of high aspect ratio, high permittivity inorganics; and 4) the electrokinetic behavior of colloidal dispersions

iii. Year 3 (JUN-2010 to AUG-2011)

- a.** Implementation and multi-scale modeling of a reconfigurable antenna demonstration vehicle using fluidic (vascular) reconfiguration mechanisms
- b.** Completed a characterization system for composites
- c.** Refined the synthesis and processing of high aspect ratio, high permittivity Barium Titanate nano-rods

5. Future Work and Follow-On Activities

This project has identified numerous unique and potentially transformative avenues of multidisciplinary research. The focus of ongoing and continuing efforts is on the development of new technologies for superconfigurable antenna systems. This includes the continued development of novel particles which can have a high impact on effective medium properties, the electrokinetic and fluidic control of these systems, and the automation of superconfigurable antenna systems with electromagnetic, thermal, and mechanical modalities.

C. Extensions Granted or Milestones Slipped

A single extension was requested and granted to change the end date of this grant from the old ending date of 30-JUN-2010 to a new ending date of 31-AUG-2011. The primary purpose of this was to ensure a full summer semester of support for the graduate students working on this project.

D. Summary of Archival Publications and Other Disseminated Work

1. Archival Publications

- [1] G. H. Huff, P. Walters, J. McDonald, and D. L. Rolando, "A reconfigurable colloidal dispersion dielectric resonator antenna," *IEEE Antennas Wireless Propag. Lett.*, vol. 9, pp. 288-290, March 2010.
- [2] G. H. Huff and S. Goldberger, "A coaxial stub microfluidic impedance transformer (COSMIX)," *IEEE Microw. Wireless Compon. Lett.*, vol. 20, pp. 154-156, March 2010.
- [3] Sanjay Kalidindi, Zoubeida Ounaies and Hamid Kaddami, 'Toward the Preparation of Nanocomposites with Oriented Fillers: Electric Field-Manipulation of Cellulose Whisker in Silicone Oil', *Smart Materials and Structures*, accepted, 2010.
- [4] Kevin Maxwell, John Whitcomb, Zoubeida Ounaies, and Amira Barhoumi, 'Finite Element Analysis of a Three-Phase Piezoelectric Nanocomposite', *Journal of Intelligent Materials System and Structures*, accepted, 2010.
- [5] Deshmukh, S. and Ounaies, Z., "Single Wall Carbon Nanotube (SWNT)-Polyimide Nanocomposites as Electrostrictive Materials", *Sensors and Actuators A: Physical*, 155, pp. 246-252, 2009.
- [6] G. H. Huff and S. A. Goldberger, "Biologically-inspired vascular antenna reconfiguration mechanism," *Electronic. Lett.* 47, 637, 2011.
- [7] F. Drummond and G. H. Huff, "Reconfiguration and thermoregulation using biologically inspired vascular networks," in *proc. European Conf. on Antennas and Propagat.* 3668, 2011.
- [8] S. A. Long and G. H. Huff, "Development of a closed-loop fluidic system for a phase reconfigurable reflectarray element," in *proc. European Conf. on Antennas and Propagat.* 1192, 2011.
- [9] S. A. Long and G. H. Huff, "A fluidic loading mechanism for phase reconfigurable reflectarray elements," *IEEE Antennas Wireless Propagat. Lett.* 10, 1, 2011.
- [10] J. J. Juarez, B. Liu, J. Cui, and M. A. Bevan, "kT-scale colloidal interactions in high frequency inhomogeneous AC electric fields. I. Single particles," *Langmuir*, (accepted) 2011
- [11] J. J. Juarez, B. Liu, J. Cui, and M. A. Bevan, "kT-scale colloidal interactions in high frequency inhomogeneous AC electric fields. II. Concentrated ensembles," *Langmuir*, (accepted) 2011
- [12] S. L. Eichmann, B. Smith, G. Meric, D. H. Fairbrother, and M. A. Bevan, "Imaging carbon nanotube interactions, diffusion, and stability in nanopores," *A.C.S. Nano.*, (accepted) 2011

2. Invited Disseminations of Work

- [1] G. H. Huff, ECE Department Seminar, University of Illinois at Urbana-Champaign, Feb. 16, 2010.
- [2] G. H. Huff, ECE Department Seminar, University of Minnesota, Feb. 4, 2010.
- [3] M. L. VanBlaricum, T. L. Larry, and G. H. Huff*, "A design approach for reconfigurable RF surfaces and apertures," *Soc. of Eng. Sci.: 45th Annu. Tech. Meeting*, Champaign, IL, Oct. 13-15, 2008.

- [4] M. A. Bevan, Colloidal Interactions and Assembly on Energy Landscapes, Chemical Engineering, City College of New York, 04.20.2009.
- [5] M. A. Bevan, Colloidal Interactions and Assembly on Energy Landscapes, Chemical Engineering, University of Louisville, 04.17.2009.
- [6] M. A. Bevan, Self- & Directed- Assembly of Interfacial Colloidal Crystals, Physics, Georgetown University, 04.03.2009.
- [7] M. A. Bevan, Colloidal Interactions and Assembly on Energy Landscapes, Chemical & Biomolecular Engineering, Rice University, 10.09.2008.
- [8] M. A. Bevan, Colloidal Interactions and Assembly on Energy Landscapes, Chemical & Biomolecular Engineering, Tulane University, 09.19.2008.
- [9] M. A. Bevan, Colloidal Interactions and Assembly on Energy Landscapes, Chemical & Biomolecular Engineering, Univ. of Pennsylvania, 09.10.2008.
- [10] M. A. Bevan, Colloidal Interactions and Assembly on Energy Landscapes, 82nd ACS Colloid and Surface Science Symposium, North Carolina State Univ., 06.17.2008.
- [11] M. A. Bevan, Colloidal Interactions and Assembly on Energy Landscapes, Chemistry, University of Maryland, Baltimore County, 04.15.2008.
- [12] M. A. Bevan, Colloidal Interactions and Assembly on Energy Landscapes, National Institute of Standards and Technology, Directed Assembly of Functional Materials and Devices, 03.19.2008.

3. Other Disseminations of Work

- [1] J. D. Barrera and G. H. Huff, "An adaptive SIW filter and dual-linearly polarized patch antenna using vertically-orientated fluidic material perturbations," accepted for NASA/ESA Conf. Adaptive Hardware Systems (June, 2010).
- [2] T.-K. Chen and G. H. Huff, "Inward-fed Archimedean spiral antenna with an internalized stripline impedance transformer and balun," accepted for IEEE/URSI Int. Symp. Antennas and Propag. (July, 2010).
- [3] D. L. Rolando and G. H. Huff, "Design trade-offs and operational perspectives of a dielectric coated spherical inverted-F antenna," accepted for IEEE/URSI Int. Symp. Antennas and Propag. (July, 2010).
- [4] S. A. Goldberger, F. Drummond, J. D. Barrera, S. Davis, J. Edelen, M. Geppert, Y. Judie, Q. Manley, C. Peters, S. Smith, and G. H. Huff, "A polarization-reconfigurable antenna using surface-integrated fluidic loading mechanisms" accepted for IEEE/URSI Int. Symp. Antennas and Propag. (July, 2010).
- [5] S. A. Long and G. H. Huff, "A Study of Nanoparticle Geometry and Material Properties in a COSMIX-Enabled Phase Reconfigurable Reflect-Array Element," accepted for IEEE/URSI Int. Symp. Antennas and Propag., June, 2010.
- [6] S. A. Long and G. H. Huff, "Integration and Performance of a COSMIX-Enabled Phase Reconfigurable Reflect-Array Element," presented at USNC-URSI Nat. Radio Sci. Meeting, Boulder, CO, Jan. 2010.
- [7] S. Goldberger, F. Drummond, J. Barrera, S. Davis, J. Edelen, M. Geppert, Y.-S. Judie, Q. Manley, C. Peters, S. Smith, and G. H. Huff, "Design of a Polarization Reconfigurable Crossed-Dipole

- Antenna using Surface Integrated Fluidic Loading Mechanisms,” presented at USNC-URSI Nat. Radio Sci. Meeting, Boulder, CO, Jan. 2010.
- [8] G. H. Huff, S. Goldberger, and S. A. Long, “Operational perspectives of biologically inspired capillary-based reconfiguration mechanisms in microstrip patch antennas,” *Antenna Applicat. Symp.*, Allerton Park, Monticello, IL, Sept. 2009.
 - [9] S. Goldberger, F. Drummond, R. Anderson, J. Barrera, A. Bolon, S. Davis, J. Edelen, J. Marshall, C. Peters, D. Umana, and G. H. Huff, “Frequency reconfiguration of a small array enabled by functionalized dispersions of colloidal materials,” 23rd Annual Conf. Small Satellites, Utah State University, Logan, UT, Aug., 2009.
 - [10] Meddeb, A. and Ounaies, Z., “Particle Size and Aspect Ratio Effects on the Dielectric Enhancement in Polymer Composites”, *Proceedings of the Society for the Advancement of Material and Process Engineering Conference (SAMPE)*, May 17-20 2010, Seattle, WA.
 - [11] Kalidindi, S., Ounaies, Z., and Kaddami, H., “Electric-Field Assisted Patterning of Cellulose Whisker-Reinforced Polymer Nanocomposites”, *Proceedings of the Society for the Advancement of Material and Process Engineering Conference (SAMPE)*, May 17-20 2010, Seattle, WA.
 - [12] Kalidindi, S., Ounaies, Z., and Kaddami, H., and Dufresne, A., “Electric Field-Manipulation of Cellulose Whisker-Reinforced Polymer Nanocomposites”, *ASME Conference on Smart Materials, Adaptive Structures and Intelligent Systems*, 21-23 September 2009, Oxnard, CA.
 - [13] Dynamic compensation mechanisms for deformable radiating structures based on colloidal dielectrics and fluidics, G. H. Huff and S. A. Long, *in proc. SPIE Smart Structures/NDE*, March, 2009.
 - [14] A Capillary-Based Reconfiguration Mechanism using Nanoparticle Dispersions for Frequency Agility in Microstrip Antenna Topologies, G. H. Huff and S. A. Goldberger, *in review. IEEE Antennas Wireless Prop. Lett.*, Submitted Aug., 2008.
 - [15] A Coaxial Stub Microfluidic Impedance Transformer (COSMIX), G. H. Huff and S. A. Goldberger, *in review. IEEE Antennas Wireless Prop. Lett.*, Submitted July., 2008.
 - [16] Electric Field Induced Colloidal Interactions & Microstructures, Juarez, J.J.; Bevan, M.A. (in preparation) 2009.
 - [17] S. A. Long and Gregory H. Huff, “Design Variations of a capillary based compensation mechanism for deformable microstrip antennas,” *in proc. 2009 IEEE/URSI Int. Symp. Antennas and Propag.*
 - [18] S. Goldberger, F. Drummond, R. Anderson, J. Barrera, A. Bolon, S. Davis, J. Edelen, J. Marshall, C. Peters, D. Umana, and G. H. Huff, “Small array behavior of frequency reconfigurable antennas enabled by functionalized dispersions of colloidal materials,” *in proc. 2009 URSI Nat. Radio Sci. Meeting*, Boulder, CO, Jan. 2009.
 - [19] D. Lagoudas, M. Bevan, G. H. Huff*, and Z. Ounaies, “Multi-scale modeling and characterization of electromagnetically tunable colloidal-based materials,” *in proc. Soc. of Eng. Sci.: 45th Annu. Tech. Meeting*, Champaign, IL, Oct. 13-15, 2008.
 - [20] *G. H. Huff, S. Goldberger, and S. A. Long, “The RF cuttlefish: Overview of biologically inspired concepts for reconfigurable antennas and smart skins” *in proc. 2008 Antenna Applicat. Symp.*, Allerton Park, Monticello, IL, Sept. 2008, pp. 291-305.
 - [21] J. McDonald and G. H. Huff*, “Microfluidic mechanisms for reconfigurable dielectric resonator antennas,” *in proc. 2008 URSI Gen. Assy.*, Chicago, IL, Aug. 2008.

- [22] S. A. Long and G. H. Huff*, "A study of microfluidic compensation mechanisms for deformable antennas," *in proc. 2008 URSI Gen. Assy.*, Chicago, IL, Aug. 2008.
- [23] *G. H. Huff, "Electromagnetically functionalized colloidal dispersions and microfluidic reconfiguration mechanisms for phase-reconfigurable reflectarray elements," *in proc. 2008 URSI Gen. Assy.*, Chicago, IL, Aug. 2008.
- [24] *Sean Goldberger and G. H. Huff, "Frequency reconfiguration of a microstrip patch antenna enabled by colloidal dispersions," *in proc. 2008 URSI Nat. Radio Sci. Meeting*, Boulder, CO, Jan. 2008.
- [25] Depletion Attraction & Electric Field Mediated Colloidal Crystal Assembly, Juarez, J.J.; Bevan, M.A. 83rd ACS Colloid and Surface Science Symposium, Columbia Univ., 06.19.2008.
- [26] Electric Field Induced Colloidal Interactions & Microstructures, Juarez, J.J.; Bevan, M.A. 83rd ACS Colloid and Surface Science Symposium, Columbia Univ., 06.16.2008.
- [27] Controlled Colloidal Assembly Via Navigation of Energy Landscapes, AIChE 2008 National Meeting, Philadelphia, PA, 11.19.2008.
- [28] Dielectrophoretic Assembly of Interfacial Colloidal Crystals, AIChE 2008 National Meeting, Philadelphia, PA, 11.19.2008.

4. Awards

- [1] Young Scientist Award, Gregory H. Huff, paper title: "Electromagnetically Functionalized Colloidal Dispersions and Microfluidic Reconfiguration Mechanisms for Phase-Reconfigurable Reflectarray Elements," presented at the 2008 General Assemblies of L'Union Radio-Scientifique Internationale (International Union of Radio Science, URSI) meeting in Chicago.

E. Changes in Research Objectives

There have been no changes in research objectives to report.

F. Change in AFOSR Program Manager

There have been no changes to report to the Program Manager of this program.